Historical and future trends in wetting and drying in 291 catchments across China

Zhongwang Chen[1,2], Huimin Lei[1,2], Hanbo Yang[1,2], Dawen Yang[1,2], and Yongqiang Cao[3]

[1]Department of Hydraulic Engineering, Tsinghua University, Beijing, 100084, China
[2]State Key Laboratory of Hydro-Science and Engineering, Tsinghua University, Beijing, 100084, China
[3]School of urban planning and Environmental science, Liaoning Normal University, Dalian, 116029, China

Correspondence to: Hanbo Yang (yanghanbo@tsinghua.edu.cn)

Abstract

An increasingly uneven distribution of hydro-meteorological factors related to climate change has been detected by global climate models (GCMs), and the pattern of changes in water availability is commonly described with the phrase "*dry gets drier, wet gets wetter*" (DDWW). However, the DDWW pattern is primarily dominated by oceanic areas, and recent studies based on both observed and modelled data have failed to verify the DDWW pattern on land. This study confirms the existence of a new DDWW pattern in China after analysing the observed streamflow data from 291 Chinese catchments from 1956 to 2000, revealing that the distribution of water resources has become increasingly uneven since 1950s. This pattern can be more accurately described as "*drier regions are more likely to become drier, whereas wetter regions are more likely to become wetter*". Based on a framework derived from the Budyko hypothesis, this study estimates runoff trends via observations of precipitation (P) and potential evapotranspiration (E_p) for the same period, finding that a high correlation exists between the estimated and observed runoff trends (R^2=0.70) and that the DDWW pattern also appropriately describes the estimated trends. Therefore, climate change has led to the historical trends in runoff as well as the DDWW pattern, with changes in P playing the most significant role. Furthermore, the P and E_p projections of five GCMs from the Coupled Model Intercomparison Project Phase 5 (CMIP5) under three scenarios (RCP2.6, RCP4.5 and RCP8.5) are used to predict the future trends in the study catchments from 2001 to 2050 based on the framework. Despite the differences among the predicted results of the different models, the DDWW pattern does not hold in the projections, regardless of the model used. Unfortunately, most areas of China (over 60%) will experience water resource shortages under the projected climate changes. Nevertheless, this conclusion remains tentative due to the large uncertainties in the GCM outputs.

1 Introduction

Terrestrial water availability is critical to human lives and economic activities (Milly et al., 2005). In recent decades, changes in water availability have had significant effects on human society (Piao et al., 2010) and the environment (Arnell, 1999) in the context of climate change. Runoff (Q) is a commonly adopted indicator of water availability (Milly et al., 2005). The response of Q to climate change has been widely investigated from the basin scale to the global scale, based on streamflow observations (e.g., Pasquini and Depetris, 2007; Dai et al., 2009; Stahl et al., 2010) or model outputs (e.g., Hamlet et al., 2007; Alkama et al., 2013; Greve et al., 2014).

Under the influence of climate change, a more uneven distribution of the hydro-meteorological elements has been detected at the global scale by the global climate models (GCMs) both spatially (Held and Soden, 2006; Chou et al., 2009) and temporally (Chou et al., 2013) as well as the observed data (Allan, 2010; Durack, 2012; Liu, 2013), resulting in probable enhancement of hydrological extremes such as floods and droughts. This response is known as the "rich-get-richer" mechanism (Chou and Neelin, 2004), from which follow-up studies derive diverse summaries of different elements, such as "*dry gets drier, wet gets wetter*" for precipitation (P) (Allan, 2010) and precipitation minus evapotranspiration ($P-E$) (Held and Soden, 2006), "*wet season gets wetter, dry season gets drier*" for seasonal precipitation (Chou et al., 2013) and "*fresh gets fresher, salty gets saltier*" for ocean salinity (Durack, 2012; Roderick et al., 2014). Furthermore, it attracts a lot of attention to explore whether there exists a similar effect in Q on land as the "*dry gets drier, wet gets wetter*" (DDWW hereinafter for short) pattern found in $P-E$, which indicates the increasingly uneven distribution of the water resources. The original DDWW pattern predicted a simple active proportional relationship between $P-E$ and $\Delta(P-E)$, as the sign of $P-E$ determines whether a region is dry (negative) or wet (positive). It should be noticed that the predicted changes were averages of latitudinal zones rather than values at the local scale (e.g., grid box or catchment), resulting in the dominance of the oceanic components in the DDWW pattern (Roderick et al., 2014), as P and E are dominated by exchanges over the ocean at most latitudes (Lim and Roderick, 2009). Thus, the DDWW pattern is more appropriately applied to the ocean than to the land. In fact, because the long-term mean $P-E$ is overwhelmingly positive on land, the method of using the sign of $P-E$ to identify wet and dry regions is not feasible anymore, as $\Delta(P-E)$ can obviously be negative. Therefore, some scholars tried to explore a new DDWW pattern to describe changes in the hydrological cycle on land at the local scale. Greve et al. (2014) adopted the aridity index (φ, $=E_p/P$, where E_p denotes the potential evapotranspiration) as a measurement of the aridity degree, and defined $\varphi>2$ as dry regions and $\varphi<2$ as wet regions. Consequently, the pattern became "$\varphi>2$, $\Delta(P-E)<0$; whereas $\varphi<2$, $\Delta(P-E)>0$". However, the results, which were based on more than 300 combinations of various global hydrologic data sets containing both observed and modelled data, showed that only 10.8% of land areas robustly followed the adjusted DDWW pattern. Nevertheless, the study of Greve et al. (2014) still has some defects related to two major aspects: one is the existence of large uncertainties in E in both the satellite-based observations and the simulations (Kumar et al., 2016), and the other is artificially assigned threshold between the wet and dry regions, which, when the threshold is changed, changes the results. Therefore, a study based on observed Q data that are more direct and of relatively low

uncertainty should be conducted as well as a new method to partition dry and wet regions not depending on the appointed threshold.

However, another problem arises in the process of studying the observed Q data: the observed changes in Q are not only responses to climate change but are also responses to other factors, such as land cover changes and human activities, e.g., withdrawal and drainage (Stahl et al., 2010). To extract the components related only to climate change is an intractable process because there is no effective method to do so. Therefore, a roundabout means is adopted by comparing the credibly estimated changes in Q under the influence of climate change with those of the observed data. Once a high correlation is verified between them, the observed changes in Q can be mainly attributed to climate change, and the presenting pattern is therefore a response to climate change. The Budyko hypothesis (Budyko, 1948) is a robust and simple tool that can accurately model mean annual Q within a catchment based only on meteorological information under climate change (Koster and Suarez, 1999). The Budyko hypothesis depicts the long-term coupled water-energy balance for a catchment as

$$\overline{E}/\overline{P} = f(\overline{E_p}/\overline{P}, c), \quad (1)$$

where the function f denotes Budyko-like equations, $\overline{E_p}$ is the mean annual potential evapotranspiration, and c is a parameter characterizing a particular catchment. There are various types of Budyko-like equations (e.g., Pike, 1964; Fu, 1981; Choudhury, 1999; Zhang et al., 2001; Yang et al., 2008; Wang and Tang, 2014; Zhou et al., 2015). The Budyko hypothesis has been examined and applied in both observation-based (Zhang et al., 2001; Oudin et al., 2008; Xu et al., 2014) and model-based studies (Zhang et al., 2008; Teng et al., 2012) and produces good consistency between observed and modelled data. By analysing hydro-meteorological data from 108 nonhumid catchments in China, Yang et al. (2007) confirmed that the Budyko hypothesis is capable of predicting Q both at long-term and annual time scales. Xiong and Guo (2012) assessed the Budyko hypothesis in 29 humid watersheds in southern China and found that parametric Budyko formulae can estimate the long-term average Q well. Therefore, the use of the Budyko hypothesis is reasonable in China. The ability to capture the effects of climate change on Q and other details of the Budyko hypothesis are described in Section 2.3.

Based on observed streamflow data from 291 catchments in China, this study first analyses the historical trends in annual Q, exploring the possible existence of a DDWW pattern via a new method proposed in Section 2.2. Then, adopting a simple framework derived from the Budyko hypothesis stated in Section 2.3, this study estimates the runoff trends caused by climate change in the study catchments, revealing that the historical trends are mainly a response to climate change and identifying the key influencing factor. Moreover, based on the Coupled Model Intercomparison Project Phase 5 (CMIP5) projections of five GCMs, this study predicts changes in Q via the framework to determine whether the DDWW pattern will continue to hold in the future.

2 Data and methods

2.1 Study area and data

This study collected hydrologic and meteorological data from 291 catchments in mainland China with drainage areas ranging from 372 to 142,963 km^2. These catchments include all the first-level basins of mainland China except the Huaihe River Basin, and their distribution is shown in **Figure 1**. Annual restored discharge data from 1956 to 2000 for each catchment outlet were provided by the Hydrological Bureau of the Ministry of Water Resources of China. Here, "restored" means the effects of human activities on the runoff in catchments, e.g., water withdrawals and reservoir regulations, have been mostly removed via certain technical means. Thus, the restored discharge can be considered the natural discharge (or very close). The records range in length from 21 years to 45 years, and 261 catchments have record lengths greater than 40 years.

Two meteorological data sets were used in this study. One is the 10 km gridded data set interpolated by Yang et al. (2014) based on 736 stations of the China Meteorological Administration, including P and potential evapotranspiration (E_p) observations from 1956 to 2000. Based on this observed data set, the annual areal P and E_p of each catchment were calculated. The other is the daily bias-corrected (see Piani et al., 2010 and Hagemann et al., 2011) modelled data set from the Inter-Sectoral Impact Model Intercomparison Project (ISI-MIP, http://www.isi-mip.org) covering the period 1951–2050, as projected by the CMIP5 under scenarios RCP2.6, RCP4.5 and RCP8.5. Historical data for each model are used up to the year 2000, and the data then split into three representative concentration pathways (RCPs). These modelled data were initially downscaled to a 0.5°×0.5° latitude–longitude grid then extracted and transformed into the ASCII format by the Institute of Environment and Sustainable Development in Agriculture, the Chinese Academy of Agricultural Sciences, China. The output data for each scenario include precipitation; mean, maximum and minimum air temperature; solar radiation; wind speed; and relative humidity for the five models (GFDL-ESM2M, HadGEM2-ES, IPSL-CM5A-LR, MIROC-ESM-CHEM and NorESM1-M). The gridded daily E_p is estimated based on the GCM outputs by the Penman Equation (Penman, 1948; see Appendix A for more details). By summing the daily P and E_p over the course of a year, this study generates annual series of P and E_p. Then, using catchment boundaries to clip the data, annual catchment-averaged P and E_p data are acquired.

2.2 Runoff trends and the DDWW pattern

In this study, two slightly different definitions of the runoff trends are adopted for the historical (1956-2000) and projected period (2001-2050). The runoff trend for the historical period is defined as the slope of the linear regression of the annual Q series, denoted by k_Q, and can be calculated by

$$k_Q = \frac{\sum_{i=1}^{m}(t_i-\bar{t})(Q_i-\overline{Q})}{\sum_{i=1}^{m}(t_i-\bar{t})^2}, \quad (2)$$

where m is the observed record length of a catchment, i is the ith record, t_i is the year of this record, $\bar{t}$ is the average of all record years, as Q_i and $\overline{Q}$ are the observed annual runoff in t_i and the mean annual runoff in historical period, respectively.

The significance of k_Q is determined using a t-test. The runoff trend of the projected period is denoted by $\Delta\overline{Q}$, defined as the change in mean annual runoff between historical and projected period, and can be computed as follows:

$$\Delta\overline{Q}=\overline{Q}_{\mathrm{p}}-\overline{Q}, \tag{3}$$

where $\overline{Q}_{\mathrm{p}}$ denotes the projected mean annual runoff. The introduction of $\Delta\overline{Q}$ is necessary because k_Q is only appropriate for an identical sample, meaning that calculating the k_Q of an integrated sample including historical and projected data is not possible. Additionally, the k_Q of only the projected period fails to describe the change between the historical and future conditions, which is contrary to our purpose. Therefore, $\Delta\overline{Q}$ is adopted as a way to compare projections with observations.

In the study of Greve et al. (2014), the DDWW pattern is sensitive to the partition between the dry and wet regions because the partition depends on an assigned threshold separating the study areas, which leads to different (possibly conflicting) results depending on different thresholds. To remove the influence of the threshold, the study of Allan et al. (2010) adopted percentile bins for P to define wet and dry regions, thereby successfully avoiding the pitfalls of selecting a convincing threshold. Therefore, this study does not define absolute "wet" or "dry" regions but instead identifies relative "wetter" or "drier" ones. To be specific, two variables are chosen to be the indicators of the aridity index, $\overline{Q}$ and φ, respectively. The term φ is introduced to maintain consistency with studies based on the climate model data where $\overline{Q}$ is not available. The spatial distribution of $\overline{Q}$ and φ are shown in **Figure 2**, with $\overline{Q}$ ranging from 0 to 1400 mm a^{-1} and φ ranging from 0.5 to 8. We divide $\overline{Q}$ and φ into six intervals, the intervals with larger $\overline{Q}$ values and smaller φ values are wetter levels. The details are listed in **Table 1**. The sum of the catchments and the number of increasingly wetter catchments in each interval are used to calculate the proportion of wetter catchments in a given interval, denoted by d. A larger d value implies that more catchments have become wetter in this level. This study compares the d values of different intervals to examine a new DDWW pattern.

2.3 A framework to estimate runoff trends under climate change

Among various types of Budyko-like equations, two analytical equations proposed by Fu (1981) and Yang et al. (2008) should be highlighted. Because these two studies each introduce a catchment property parameter, ω and n, respectively (two examples of c in Equation (1)), the two equations are able to better capture the role of landscape characteristics. Yang et al. (2008) showed a high linear correlation between ω and n. Therefore, this study chooses the equation derived by Yang et al. (2008), which has been rewritten as follows:

$$\frac{\overline{E}}{\overline{P}}=\left[\left(\frac{\overline{E}_{\mathrm{p}}}{\overline{P}}\right)^{-n}+1\right]^{-1/n}. \tag{4}$$

Focusing on Q, this study transforms Equation (4) into

$$\overline{Q}=\overline{P}-\overline{P}\left[\left(\frac{\overline{E}_{\mathrm{p}}}{\overline{P}}\right)^{-n}+1\right]^{-1/n}. \tag{5}$$

The parameter n can be calculated using the observed $\overline{Q}$, $\overline{P}$ and $\overline{E_p}$ of each catchment from the period of 1956 to 2000. The differential form of Equation (5) is derived as follows:

$$dQ = \frac{\partial Q}{\partial P} dP + \frac{\partial Q}{\partial E_p} dE_p + \frac{\partial Q}{\partial n} dn, \quad (6)$$

where dQ, dP, dE_p and dn denote deviations in the observed or modelled Q, P, E_p and n with respect to long-term mean value. Equation (6) has widely been used to estimate changes in annual Q (e.g., Yang and Yang, 2011; Roderick and Farquhar, 2011; Roderick et al., 2014).

Since we focus on the effects of climate change, n is assumed to remain unchanged, i.e., dn equalling 0 (Yang and Yang, 2011), and Equation (6) becomes

$$dQ = \frac{\partial Q}{\partial P} dP + \frac{\partial Q}{\partial E_p} dE_p. \quad (7)$$

For convenience, we introduce ε_P and ε_0 to represent $\frac{\partial Q}{\partial P}$ and $\frac{\partial Q}{\partial E_p}$, which can be estimated based on n, $\overline{P}$ and $\overline{E_p}$:

$$\varepsilon_P = \left.\frac{\partial Q}{\partial P}\right|_{(\overline{P},\overline{E_p})} = 1 - \left[1 + \left(\frac{\overline{E_p}}{\overline{P}}\right)^{-n}\right]^{\frac{n+1}{n}} \text{ and}$$

$$\varepsilon_0 = \left.\frac{\partial Q}{\partial E_p}\right|_{(\overline{P},\overline{E_p})} = -\left[1 + \left(\frac{\overline{E_p}}{\overline{P}}\right)^{n}\right]^{\frac{n+1}{n}}.$$

Roderick et al. (2014) showed that the runoff changes (=$\Delta(P - E)$ in this study) estimated using Equation (7) account for around 82% of the variation in the GCM projections of $\Delta(P - E)$. Therefore, Equation (7) can predict a reliable result under climate change projected by GCMs. Based on Equation (7), a framework can then be constructed to estimate runoff trends (see Appendix B for interpretation):

$$k_{Qe} = \varepsilon_P k_P + \varepsilon_0 k_{E_p}, \quad (8a)$$

$$\Delta\overline{Q}_e = \varepsilon_P \Delta\overline{P} + \varepsilon_0 \Delta\overline{E_p}, \quad (8b)$$

where k_{Qe} and $\Delta\overline{Q}_e$ are estimated runoff trends of the historical and projected period, respectively; k_P and k_{E_p} are the linear regression-calculated trends in annual P and E_p, respectively; and $\Delta\overline{P}$ and $\Delta\overline{E_p}$ are changes in $\overline{P}$ and $\overline{E_p}$, respectively.

Equations (8a) and (8b) attribute the runoff trend to two major factors, the precipitation trend and the potential evapotranspiration trend. Equation (8a) estimates k_{Qe} according to the observed k_P and k_{E_p}. Equation (8b) estimates $\Delta\overline{Q}_e$ according to the GCM projections, and $\Delta\overline{P}$ and $\Delta\overline{E_p}$ are calculated as differences in $\overline{P}$ and $\overline{E_p}$ between 1956–2000 and 2001–2050. Due to the uncertainty of the GCMs, the coefficient of variance (C_v) in each catchment is estimated. The C_v is defined as the ratio between the standard deviation and the absolute mean of the five $\Delta\overline{Q}_e$ outputs of the respective GCMs. Specifically, a lower C_v indicates less uncertainty in $\Delta\overline{Q}_e$ because the results of the different GCMs are similar.

3 Results and discussion

3.1 Historical trends in annual runoff

Figure 3 presents the spatial distribution of observed k_Q in the 291 study catchments. At the significance level of 0.05, 39.9% (116 of 291) of the study catchments are undergoing significant changes in annual Q and are called "significant catchments" in the following text. Trends towards wetter conditions (positive trends) are found mainly in the upper and lower reaches of the Yangtze River basin, the Southwest and the Southeast Rivers basin, the Pearl River basin and the Inland Rivers basin. The annual Q in the lower reaches of the Yangtze River basin and the Northern Xinjiang Uygur Autonomous Region is robustly increasing by over 2 mm a^{-1}, which is greater than the rates of most other catchments. The largest increasing trend of 10.3 mm a^{-1} is observed in the Yangtze River basin. However, the catchments in the middle reaches of the Yangtze River basin and in northern and northeastern China are experiencing the greatest reductions in runoff, generally with significant trends. Several catchments have negative trends of over 4 mm a^{-1}, and the most severe situation is in the Yellow River basin, where the annual Q is decreasing at a rate of 7.2 mm a^{-1}.

The relationship between k_Q and $\overline{Q}$ is plotted in **Figure 4**, which also shows the d for each interval. With increasing $\overline{Q}$, d increases from 0.18 to 0.88, meaning that "*drier regions are more likely to become drier, whereas wetter regions are more likely to become wetter*". The slight decrease in d to 0.79 in the last interval can be attributed to the small sample size of this interval, as the number of catchments getting drier is actually equal in intervals 5 and 6 (**Table 2**). Therefore, a new DDWW pattern is derived based on the analysis of the observed data. This pattern emphasizes the fact that the distribution of water resources has become more uneven in China since 1950s. The process driving the uneven distribution of water resources in this study is powerful because nearly all the wettest catchments became wetter and the driest catchments became drier.

Moreover, to introduce the DDWW pattern into studies based on climate model data where $\overline{Q}$ is not available, an analysis of k_Q and φ is also performed. **Figure 5** shows that d decreases from 0.86 to 0.16 as φ increases, implying that the DDWW pattern also holds if we adopt φ to describe the aridity degree, similar to Greve et al. (2014). This relationship is explained by **Figure 6a**, in which a monotonic decrease in $\overline{Q}$ with φ is revealed. However, d increases sharply to 0.36 in the last interval, in contrast to the DDWW pattern. To understand this divergence, we have marked areas with φ>2 and k_Q>0 (26 in total) in **Figure 6b**. Surprisingly, most of these areas (19 of 26) are located in areas with glaciers. Therefore, the changes in water storage (ΔS) from the melting of glacial ice and snow also play a key role in the runoff generation there. However, φ does not consider the influence of ΔS, thereby leading to an overestimation of the aridity degree in these catchments, i.e., they are in the wrong intervals. This reflects the weakness of the ability of φ to assess the aridity degree with respect to water resources compared to $\overline{Q}$. Moreover, if we can acquire specific ΔS information, by redefining an adjustable aridity index (φ') as $(P - \Delta S)/E_p$, the failure of the DDWW pattern in areas with high φ is not expected to exist anymore.

The finding of the DDWW pattern in China has led us to review the study of Greve et al. (2014) and realize the probability of the worldwide existence of the DDWW pattern. Based on a threshold (φ=2) to identify wet and dry regions,

Greve et al. noted that the traditional summary "*dry get drier, wet get wetter*" does not hold over land between the periods 1948-1968 and 1985-2005. After removing transitional areas that cannot be definitely identified as wet or dry, the percentages of the four types, i.e., wet-wetter (WW), wet-drier (WD), dry-wetter (DW) and dry-drier (DD), computed via Figure 4c for the residual areas (Greve et al., 2014) are 21%, 42%, 5% and 32%, respectively. Unfortunately, Greve et al. did not provide detailed information on φ for the study regions, and we therefore cannot examine the DDWW pattern directly as we did for the observed data. However, to elucidate the possibility of the DDWW pattern over land, we can simply assume a special situation as in **Figure 7**. Each shape denotes one type of regions (WW, WD, DW and DD) in Greve et al. (2014), and the area in a small interval represents the count of respective regions, with the total area representing the sum of this type. In this situation, the DDWW pattern apparently holds as d decreases when φ increases. Certainly, to ensure the existence of the DDWW pattern globally, a subsequent study that includes the distribution of φ across the world is necessary.

3.2 Interpreting the trends from climate change perspective

Based on a comparison of the Budyko-estimated $k_{Q\mathrm{e}}$ with observed k_Q, the coefficients of determination (R^2) (Legates and McCabe, 1999) are 0.70 and 0.86 for all catchments and for significant catchments, respectively (**Figure 8**).Therefore, the majority of the runoff trends can be attributed to changes in the atmospheric forcing of water and energy. However, the slope k is smaller than one (0.60 and 0.62 for all catchments and significant catchments, respectively), implying that the Budyko-based framework underestimates the changes in runoff. Since the framework only quantifies the effects of climate change, the estimated deviation may stem from the neglect of other influencing factors, such as ecological and environmental changes, that result in changes in the catchment properties (dn in Equation 6) that we assume to be constant in this study. Nevertheless, despite underestimating the runoff trends, the framework can correctly note the direction of runoff changes in more than 80% of the study catchments (**Figure 8**), as the error rates (proportions of misestimated catchments that have different signs of observed and estimated trends) in all and significant catchments are 18.6% (54 of 291) and 6.0% (7 of 116), respectively. Furthermore, the DDWW pattern works well based on $k_{Q\mathrm{e}}$ (**Figure 9**), which validates the DDWW pattern from the perspective of climate change based on historical meteorological observations. It also indicates the feasibility of using only P and E_p information to examine the pattern, and serves as a reference for studies based on climate model outputs.

In catchments where the observed and estimated signs are consistent, the parts of $k_{Q\mathrm{e}}$ generated from P (k_Q^P, $=\varepsilon_P k_P$) and E_p (k_Q^0, $=\varepsilon_0 k_{E_\mathrm{p}}$) are compared to find the factor controlling the runoff changes due to climate change. As shown in **Figure 10**, k_P makes an overwhelming contribution in 88.6% (210 of 237) of these catchments, as ratios of absolute k_Q^0 to absolute k_Q^P are smaller than 1. This result can add an instance to the study of Roderick et al. (2014) based on the GCM outputs (CMIP3), of which a significant conclusion is that the changes in water availability ($\Delta(P-E)$) are dominated by the changes in P (ΔP) globally. Moreover, when linking k_P with $\overline{Q}$ (**Figure 11**), we observe a pattern similar to the DDWW pattern, i.e., "more precipitation in wetter areas, and less in drier areas". This pattern is the result of the dominant position of k_P and the positive

effect of k_P on the runoff trends. Therefore, from the perspective of climate change, the more uneven precipitation results in more uneven runoff, producing the DDWW pattern.

3.3 Predicting future trends using the GCM projections

Based on the GCM projections, equation (8b) predicts the future runoff trends $\Delta\overline{Q}_e$ between the periods of 1956–2000 and 2001–2050. The results show that great discrepancies appear in $\Delta\overline{Q}_e$ among the five GCMs even under the same scenario, whereas the model-averaged results under different scenarios are close (**Figure 12**). The C_v values of $\Delta\overline{Q}_e$ in each catchment are presented in **Figure 13**. Taking the RCP2.6 scenario as an example, over two-fifths (41.9%) of the catchments have a C_v value larger than 0.5, which is indicative of considerable uncertainty in the various models reported by previous studies (e.g., Greve et al., 2014; Kumar et al., 2016). However, the proposed DDWW pattern is no longer suitable under three scenarios, regardless of which model is selected, because d decreases as $\overline{Q}$ increases, except for an increase in interval 6, in contrast to the DDWW pattern. It can be speculated that the failure of the DDWW pattern doesn't mean an obvious alleviation of the uneven water resource distribution but conveys a bad news that most areas of China (over 60%, calculated from **Table 3**) will experience water resource shortages under the projected climate changes, whereas the changes in the conditions of the driest (interval 6) and wettest (interval 1) areas are relatively slight. Furthermore, a process similar to that described in Section 3.2 is performed to identify the main meteorological factor controlling the future trends. As shown in **Figure 14**, trends in P ($\Delta\overline{P}$) are no longer the controlling factor, as only 40% of the catchments have values of $\left|\frac{\varepsilon_0\Delta\overline{E_p}}{\varepsilon_P\Delta\overline{P}}\right|$ smaller than 1. Note that this result is based on the mean values of the five GCMs.

The spatial distribution of model-averaged relative changes in $\overline{Q}$ ($\Delta\overline{Q}_e/\overline{Q}$) is shown in **Figure 15**. The results under the three scenarios are similar. Red regions are catchments where $\overline{Q}$ will fall by more than 60% relative to the historical value, and most of these regions are located in the Yellow River Basin with relatively high certainty (C_v<0.5). The most severe situation arises in a catchment situated in the Yangtze River Basin, where the runoff is predicted to be nearly zero and the C_v is less than 0.2. In contrast, dark blue areas are catchments where $\overline{Q}$ is projected to increase by over 40%. These catchments are primarily located in the Inland River Basin, except for Northwest China, where catchments will suffer from a shortage of fresh water. Instead of continuing to become drier, catchments in Northeast and North China are projected to generate more runoff in the future, whereas catchments in the lower reaches of the Yangtze River Basin will experience considerable reductions in runoff, despite historical increases. These are the most obvious distinctions between the projected and historical runoff changes. Thus, the DDWW pattern fails to accurately characterize these future patterns.

However, an inevitable concern about the GCM outputs is their uncertainty, which determines the reliability of the projected results. To examine the uncertainty, one workable method is to compare meteorological observations with simulations for the period of 1956–2000. Taking the results of the GFDL-ESM2M model as an example (**Figure 16**), $\overline{P}$ is simulated well except for some obvious incorrectly estimated points far from the $y = x$ line. However, simulations of $\overline{E_p}$

show tremendous deviations, resulting in no obvious linear relationship between the simulated and observed values. This simple comparison directly highlights the unreliability of the GCM outputs. Although uncertainties also exist in observations due to observational errors associated with the relevant variables, such as air temperature, solar radiation and wind speed, the obvious differences between the observed and simulated values of $\overline{E_p}$ should be mainly attributed to the GCM outputs. These findings also demonstrate that further improvements in the GCMs are necessary.

4 Conclusions

Based on the analysis of restored streamflow in 291 catchments across China from 1956 to 2000, wetting trends were found mainly in the upper and lower reaches of the Yangtze River basin, Southwest and Southeast China and the Inland River basin, whereas drying trends were found in the catchments in the middle reaches of the Yangtze River basin and in North and Northeast China. By relating k_Q to $\overline{Q}$, a suitable DDWW pattern is revealed: "*drier regions are more likely to become drier, whereas wetter regions are more likely to become wetter*", implying that the distribution of the water resources in China has become more uneven since the 1950s. This study adopts φ as an indicator of water availability, which is similar to most researches on climate change based on GCMs, and validates the DDWW pattern in all the catchments except for those located in glacier regions with large φ values, where ΔS plays a significant role in the runoff generating. Moreover, as seen from the perspective of the new DDWW pattern, the study of Greve et al. (2014) may also support this finding, and the uneven trend is likely a global phenomenon.

A framework based on the Budyko hypothesis was introduced to interpret the DDWW pattern from the perspective of climate change. The high correlation between k_{Qe} and k_Q demonstrates that the runoff changes can be mainly attributed to the changes in the atmospheric forcing of water and energy. Although the framework underestimated the trends, possibly due to the neglect of other natural factors leading to catchment property changes, it can correctly indicate the direction of runoff changes in more than 80% of the study catchments. Additionally, the DDWW pattern is applicable based on k_{Qe}, indicating the feasibility of using the framework to assess the pattern. Furthermore, this framework reveals that k_P is the controlling factor associated with climate change, and the finding of a pattern similar to the DDWW pattern in k_P indicates that increasingly uneven precipitation results in increasingly uneven runoff.

According to the projections of five GCMs (GFDL-ESM2M, HadGEM2-ES, IPSL-CM5A-LR, MIROC-ESM-CHEM and NorESM1-M) from CMIP5, this study predicted future changes in $\overline{Q}$ under three scenarios (RCP2.6, RCP4.5 and RCP8.5). Significant differences are present among the different models. However, the proposed DDWW pattern is no longer suitable, regardless of which model is selected, as the proportion of catchments becoming wetter decreases as $\overline{Q}$ increases. Unfortunately, the model-average results suggest that over 60% of catchments will experience water resource shortages under future climate change, and the P trends ($\Delta\overline{P}$) will no longer be the controlling factor in runoff changes, as only 40% of the study catchments will be primarily controlled by $\Delta\overline{P}$, which is different from the phenomenon that the runoff change was

controlled by precipitation in about 90% catchments in the historical period. The catchments in Northeast and North China, which were becoming drier, will generate more runoff in the future, whereas the catchments in the lower reaches of the Yangtze River Basin, which were becoming wetter, will experience considerable reductions in runoff. These changes represent the most obvious differences between the projected and historical runoff changes. Thus, the DDWW pattern fails to explain the future changes. Nevertheless, the above conclusions remain tentative due to the enormous unreliability of the GCM outputs as indicated by the extremely low correlations between the simulated and observed $\overline{E_p}$ values for the period of 1956–2000.

Acknowledgements

This research was partially supported by funding from the National Natural Science Foundation of China (Grant Nos. 51622903 and 51379098), the National Program for Support of Top-notch Young Professionals, and the Program from the State Key Laboratory of Hydro-Science and Engineering of China (Grant No. sklhse-2016-A -02).

References

Alkama, R., Marchand, L., Ribes, A., and Decharme, B.: Detection of global runoff changes: results from observations and CMIP5 experiments, Hydrol. Earth Syst. Sci., 17, 2967-2979, doi:10.5194/hess-17-2967-2013, 2013.

Allan, R. P., Soden, B. J., John, V. O., Ingram, W., and Good, P.: Current changes in tropical precipitation, Envirom. Res. Lett., 5,doi:, 10.1088/1748-9326/5/2/025205, 2010.

Arnell, N. W.: Climate change and global water resources, Glob. Environ. Change, 9, S31-S49, 1999.

Budyko, M. I.: Evaporation under Natural Conditions, Israel Program for Scientific Translations, Jerusalem, 1948.

Chou, C., and Neelin, J. D.: Mechanisms of global warming impacts on regional tropical precipitation, J. Climate, 17, 2688-2701,doi:, 10.1175/1520-0442(2004)017<2688:MOGWIO>2.0.CO;2, 2004.

Chou, C., Neelin, J. D., Chen, C., and Tu, J.: Evaluating the "Rich-Get-Richer" Mechanism in Tropical Precipitation Change under Global Warming, J. Climate, 22, 1982-2005,doi:, 10.1175/2008JCLI2471.1, 2009.

Chou, C., Chiang, J. C. H., Lan, C., Chung, C., Liao, Y., and Lee, C.: Increase in the range between wet and dry season precipitation, Nat. Geosci., 6, 263-267, doi:10.1038/ngeo1744, 2013.

Choudhury, B. J.: Evaluation of an empirical equation for annual evaporation using field observations and results from a biophysical model, J. Hydrol., 216, 99-110, doi:10.1016/S0022-1694(98)00293-5, 1999.

Dai, A., Qian, T., Trenberth, K. E., and Milliman, J. D.: Changes in continental freshwater discharge from 1948 to 2004, J. Climate, 22, 2773-2792, doi:10.1175/2008JCLI2592.1, 2009.

Durack, P. J., Wijffels, S. E., and Matear, R. J.: Ocean Salinities Reveal Strong Global Water Cycle Intensification During 1950 to 2000, Science, 336, 455-458,doi:, 10.1126/science.1212222, 2012.

Fu, B.: On the calculation of the evaporation from land surface, Scienta Atmos. Sinica, 5, 23–31, 1981.

Greve, P., Orlowsky, B., Mueller, B., Sheffield, J., Reichstein, M., and Seneviratne, S. I.: Global assessment of trends in wetting and drying over land, Nat. Geosci., 7, 716-721, doi:10.1038/ngeo2247, 2014.

Guo, W., Liu, S., Yao, X., Xu, J., Shangguan, D., Wu, L., Zhao, J., Liu, Q., Jiang, Z., Wei, J., Bao, W., Yu, P., Ding, L., Li, G., Li, P., Ge, C. and Wang, Y.: The second glacier inventory dataset of China (Version 1.0). Cold and Arid Regions Science Data Center at Lanzhou, doi:10.3972/glacier.001.2013.db, 2014.

Hagemann, S., Chen, C., Haerter, J. O., Heinke, J., Gerten, D., and Piani, C.: Impact of a statistical bias correction on the projected hydrological changes obtained from three GCMs and two hydrology models, J. Hydrometeorol, 12, 556–578, 2011.

Hamlet, A. F., Mote, P. W., Clark, M. P., and Lettenmaier, D. P.: Twentieth-century trends in runoff, evapotranspiration, and soil moisture in the Western United States, J. Climate, 20, 1468–1486, doi:10.1175/JCLI4051.1, 2007.

Held, I. M. and Soden, B. J.: Robust responses of the hydrological cycle to global warming, J. Climate, 19, 5686-5699, doi:10.1175/JCLI3990.1, 2006.

Koster, R. D. and Suarez, M. J.: A simple framework for examining the interannual variability of land surface moisture fluxes, J. Climate, 12, 1911–1917, doi:10.1175/1520-0442(1999)012<1911:ASFFET>2.0.CO;2, 1999.

Kumar, S., Zwiers, F., Dirmeyer, P. A., Lawrence, D. M., Shrestha, R., and Werner, A. T.: Terrestrial contribution to the heterogeneity in hydrological changes under global warming, Water Resour. Res., 52, 3127-3142, doi:10.1002/2016WR018607, 2016.

Legates, D. R. and McCabe, G. J.: Evaluating the use of "goodness-of-fit" measures in hydrologic and hydroclimatic model validation, Water Resour. Res., 35, 233-241, doi:10.1029/1998WR900018, 1999.

Lim, W. H. and Roderick, M. L.: An atlas of the global water cycle: based on the IPCC AR4 Models, Australian National University Press, Canberra, 2009.

Liu, C., and Allan, R. P.: Observed and simulated precipitation responses in wet and dry regions 1850-2100, Environ. Res. Lett., 8,doi:, 10.1088/1748-9326/8/3/034002, 2013.

Milly, P. C. D., Dunne, K. A., and Vecchia, A. V.: Global pattern of trends in streamflow and water availability in a changing climate, Nature, 438, 347-350, doi:10.1038/nature04312, 2005.

Oudin, L., Andréassian, V., Lerat, J., and Michel, C.: Has land cover a significant impact on mean annual streamflow? An international assessment using 1508 catchments, J. Hydrol., 357, 303-316, doi:10.1016/j.jhydrol.2008.05.021, 2008.

Pasquini, A. I. and Depetris, P. J.: Discharge trends and flow dynamics of South American rivers draining the southern Atlantic seaboard: an overview, J. Hydrol., 333, 385-399, doi:10.1016/j.jhydrol.2006.09.005, 2007.

Penman, H. L.: Natural evaporation from open water, bare soil and grass, Proc. Royal Soc. A Math. Phys. Eng. Sci., 193, 120–145, doi:10.1098/rspa.1948.0037, 1948.

Piani, C., Weedon, G. P., Best, M., Gomes, S. M., Viterbo, P., Hagemann, S., and Haerter, J. O.: Statistical bias correction of global simulated daily precipitation and temperature for the application of hydrological models, J. Hydrol., 395, 199–215, 2010.

Piao, S., Ciais, P., Huang, Y., Shen, Z., Peng, S., Li, J., Zhou, L., Liu, H., Ma, Y., Ding, Y., Friedlingstein, P., Liu, C., Tan, K., Yu, Y., Zhang, T., and Fang, J.: The impacts of climate change on water resources and agriculture in China, Nature, 467, 43-51, doi:10.1038/nature09364, 2010.

Pike, J. G.: The estimation of annual run-off from meteorological data in a tropical climate, J. Hydrol., 2, 116-123, 1964.

Roderick, M. L., Farquhar, G. D.: A simple framework for relating variations in runoff to variations in climatic conditions and catchment properties, Water Resour. Res., 47, doi:10.1029/2010WR009826, 2011.

Roderick, M. L., Sun, F., Lim, W. H., and Farquhar, G. D.: A general framework for understanding the response of the water cycle to global warming over land and ocean, Hydrol. Earth Syst. Sci., 18, 1575–1589, doi:10.5194/hess-18-1575-2014, 2014.

Stahl, K., Hisdal, H., Hannaford, J., Tallaksen, L. M., van Lanen, H. A. J., Sauquet, E., Demuth, S., Fendekova, M., and Jódar, J.: Streamflow trends in Europe: evidence from a dataset of near-natural catchments, Hydrol. Earth Syst. Sci., 14, 2367-2382, doi:10.5194/hess-14-2367-2010, 2010.

Teng, J., Chiew, F. H. S., Vaze, J., Marvanek, S., and Kirono, D. G. C.: Estimation of climate change impact on mean annual runoff across continental Australia using Budyko and Fu equations and hydrological models, J. Hydrometeor, 13, 1094-1106, doi:10.1175/JHM-D-11-097.1, 2012.

Wang, D. and Tang, Y.: A one-parameter Budyko model for water balance captures emergent behavior in Darwinian hydrologic models, Geophys. Res. Lett., 41, 4569-4577, 2014.

Xiong, L. and Guo, S.: Appraisal of Budyko formula in calculating long-term water balance in humid watersheds of southern China, Hydrol. Process., 26, 1370–1378, doi:10.1002/hyp.8273, 2012.

Xu, X., Yang, D., Yang, H., and Lei, H.: Attribution analysis based on the Budyko hypothesis for detecting the dominant cause of runoff decline in Haihe basin, J. Hydrol., 510, 530-540, doi:10.1016/j.jhydrol.2013.12.052, 2014.

Yang, D., Sun, F., Liu, Z., Cong, Z., Ni, G., and Lei, Z.: Analyzing spatial and temporal variability of annual water-energy balance in nonhumid regions of China using the Budyko hypothesis, Water Resour. Res., 43, doi:10.1029/2006WR005224, 2007.

Yang, H., Yang, D., Lei, Z., and Sun, F.: New analytical derivation of the mean annual water-energy balance equation, Water Resour. Res., 44, doi:10.1029/2007WR006135, 2008.

Yang, H., Yang, D.: Derivation of climate elasticity of runoff to assess the effects of climate change on annual runoff, Water Resour. Res., 47, doi:10.1029/2010WR009287, 2011.

Yang, H., Qi, J., Xu, X., Yang, D., and Lv, H.: The regional variation in climate elasticity and climate contribution to runoff across China, J. Hydrol., 517, 607-616, doi:10.1016/j.jhydrol.2014.05.062, 2014.

Zhang, L., Dawes, W. R., and Walker, G. R.: Response of mean annual evapotranspiration to vegetation changes at catchment scale, Water Resour. Res., 37, 701-708, doi:10.1029/2000WR900325, 2001.

Zhang, L., Potter, N., Hickel, K., Zhang, Y., and Shao, Q.: Water balance modeling over variable time scales based on the Budyko framework – model development and testing, J. Hydrol., 360, 117-131, doi:10.1016/j.jhydrol.2008.07.021, 2008.

Zhou, S., Yu, B., Huang, Y., and Wang, G.: The complementary relationship and generation of the Budyko functions, Geophys. Res. Lett., 42, 1781-1790, 2015.

Appendix A

The procedure for using the Penman Equation to estimate E_p (mm d^{-1}) based on the GCM outputs is described in detail in this appendix. The Penman Equation can be written as (Yang et al., 2011)

$$E_p=\frac{0.408\Delta(R_n-G)+2.624\gamma(1+0.536u_2)(1-\mathrm{RH})e_s}{\Delta+\gamma}, \quad (A.1)$$

where e_s is the saturated vapor pressure (kPa), Δ is the slope of the saturated vapour pressure versus air temperature curve (kPa °C^{-1}) when the saturated vapour pressure equals e_s, R_n is the net radiation (MJ m^{-2} d^{-1}), G is the soil heat flux (MJ m^{-2} d^{-1}), γ is a psychometric constant (kPa °C^{-1}), u_2 is the wind speed at a height of 2 m (m s^{-1}), and RH is the relative humidity (%) (Yang et al., 2011).

The form of the saturated vapour pressure versus air temperature curve is

$$e(T)=0.6108\exp\left(\frac{17.27T}{T+237.3}\right), \quad (A.2)$$

where T denotes the daily air temperature, and e_s of the day can be calculated by

$$e_s=\frac{e(T_{max})+e(T_{min})}{2}, \quad (A.3)$$

where T_{max} and T_{min} are maximum and minimum daily air temperatures, respectively.

The GCM outputs are daily T_{max}, T_{min} (which can be used to calculate e_s and Δ), u_2 and RH. Assuming G equals 0 and if we compute R_n, we can use Equation (A.1) to estimate E_p. The process of utilizing the solar radiation (R_s) to compute R_n is described below.

Firstly, we calculate the incoming net short wave radiation (R_{ns}) by

$$R_{ns}=(1-\alpha)R_s, \quad (A.4)$$

where α denotes the albedo.

Next, the net outgoing long-wave radiation (R_{nl}) is estimated by

$$R_{nl}=\sigma\left(\frac{T_{max}^4+T_{min}^4}{2}\right)\left(0.34-0.14\sqrt{e_a}\right)\left(1.35\frac{R_s}{R_{s0}}-0.35\right), \quad (A.5)$$

where σ is the Stefan–Boltzmann constant (=4.903×10^{-9} MJ K^{-4} m^{-2} day^{-1}), e_a is the actual vapour pressure (=$e_s \times$ RH), and R_{s0} is the clear-sky solar radiation, which can be computed by

$$R_{s0}=(0.75+2\times10^{-5}z)R_a, \quad (A.6)$$

where z is the station elevation above sea level (m), which is available from the GCMs, and R_a is the extraterrestrial radiation (MJ m^{-2} d^{-1}) determined by Equations (21) to (25) in Allen et al. (1998).

Finally, by subtracting R_{nl} from R_{ns}, we obtain R_n.

Appendix B

This appendix provides an explicit description of the derivation of the framework for estimating k_Q and $\Delta\overline{Q}$ from Equation (8). Substituting Equation (8) into Equation (2) yields

$$k_Q = \frac{\sum_{i=1}^{m}(t_i-\bar{t})(\varepsilon_P \Delta P_i + \varepsilon_0 \Delta E_{\mathrm{p}i})}{\sum_{i=1}^{m}(t_i-\bar{t})^2}. \quad \text{(B.1)}$$

This equation can be transformed into

$$k_Q = \varepsilon_P \frac{\sum_{i=1}^{m}(t_i-\bar{t})\Delta P_i}{\sum_{i=1}^{m}(t_i-\bar{t})^2} + \varepsilon_0 \frac{\sum_{i=1}^{m}(t_i-\bar{t})\Delta E_{\mathrm{p}i}}{\sum_{i=1}^{m}(t_i-\bar{t})^2}. \quad \text{(B.2)}$$

Recalling the definition of the trend in this study, Equation (B.2) can be considered a linear combination of k_P and $k_{E_{\mathrm{p}}}$:

$$k_Q = \varepsilon_P k_P + \varepsilon_0 k_{E_{\mathrm{p}}}.$$

Equation (3) can be rewritten as

$$\Delta\overline{Q} = \frac{\sum_{i=1}^{m} Q_{\mathrm{p}i} - m\bar{Q}}{m}. \quad \text{(B.3)}$$

Recombination of the variables leads to the following expression:

$$\Delta\overline{Q} = \frac{\sum_{i=1}^{m}(Q_{\mathrm{p}i} - \bar{Q})}{m}. \quad \text{(B.4)}$$

Similarly, the substitution of Equation (8) yields

$$\Delta\overline{Q} = \frac{\sum_{i=1}^{m}(\varepsilon_P \Delta P_i + \varepsilon_0 \Delta E_{\mathrm{p}i})}{m}. \quad \text{(B.5)}$$

We finally obtain the target equation:

$$\Delta\overline{Q} = \varepsilon_P \Delta\overline{P} + \varepsilon_0 \Delta\overline{E_{\mathrm{p}}}.$$

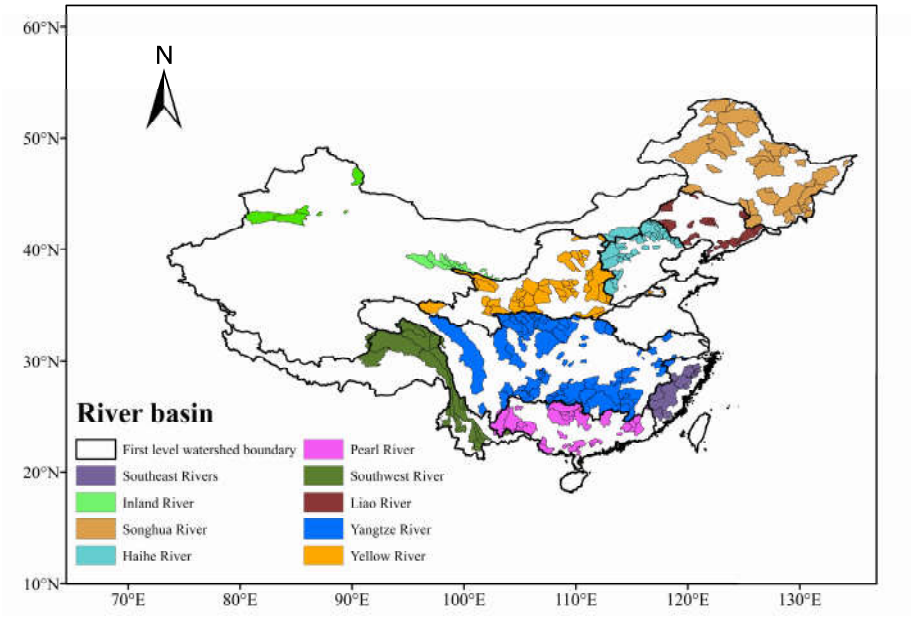

Figure 1: Spatial distribution of the 291 study catchments across mainland China.

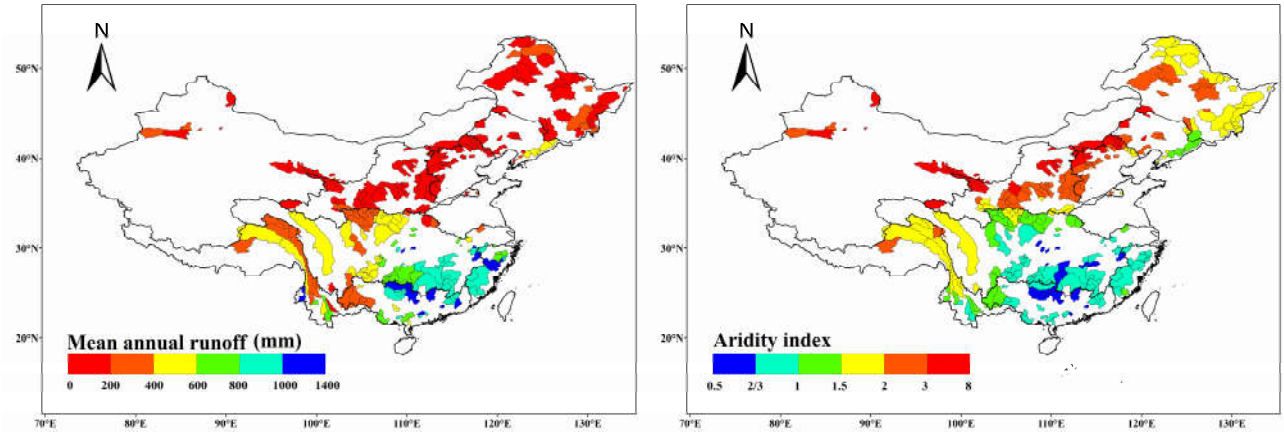

Figure 2: Spatial distribution of mean annual runoff $\overline{Q}$ (left) and aridity index φ (right) in the 291 study catchments.

5

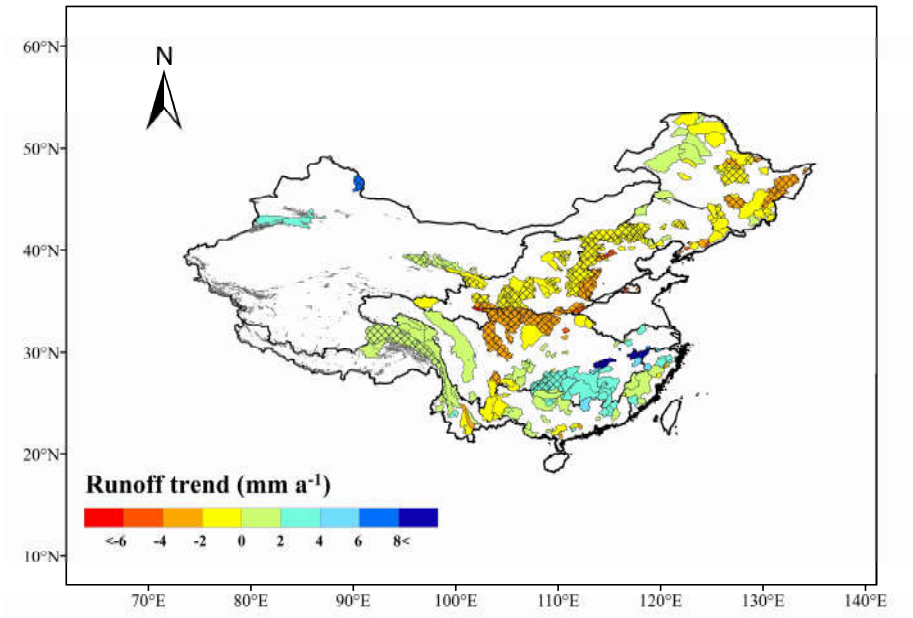

Figure 3: The observed runoff trends (k_Q) in the 291 catchments for the period of 1956 to 2000. Dark red and blue denote catchments with a trend smaller than -6 mm a^{-1} and larger than 8 mm a^{-1}, respectively. Crosshatched areas are significant catchments (p7). Grey shaded areas are glaciers based on the second glacier inventory data set of China (Guo et al., 2014).

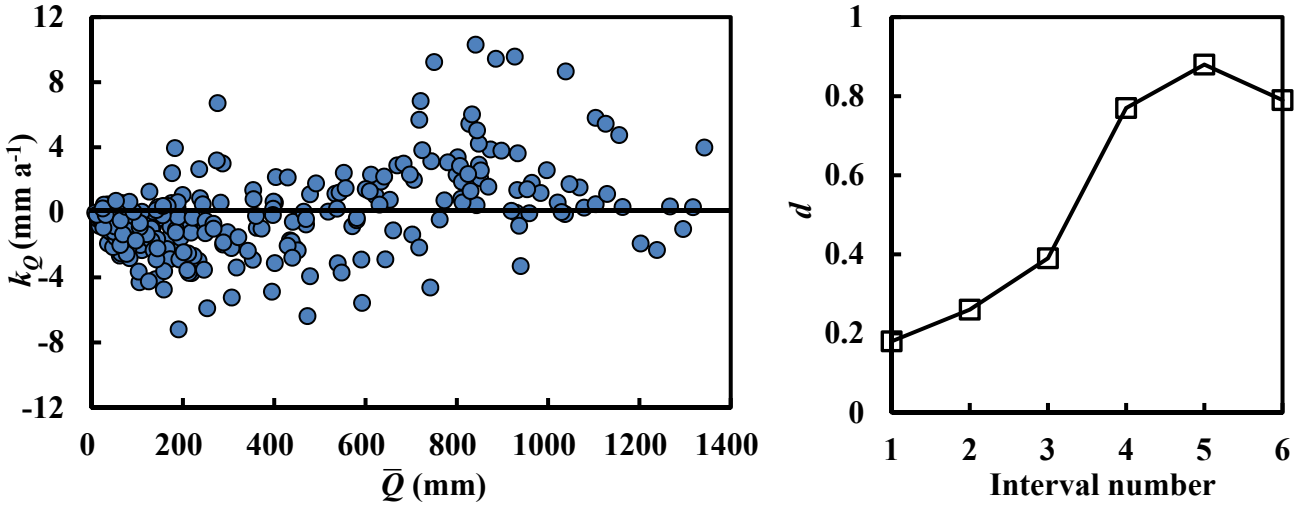

Figure 4: Relationship between observed runoff trends k_Q and mean annual runoff $\overline{Q}$ for the study catchments (left) and values of *d* in each interval according to $\overline{Q}$ (right). *d* denotes the proportion of catchments with positive trends in each interval. Interval numbers 1 to 6 correspond to six intervals 0–200, 200–400, 400–600, 600–800,800–1000 and 1000–1400.

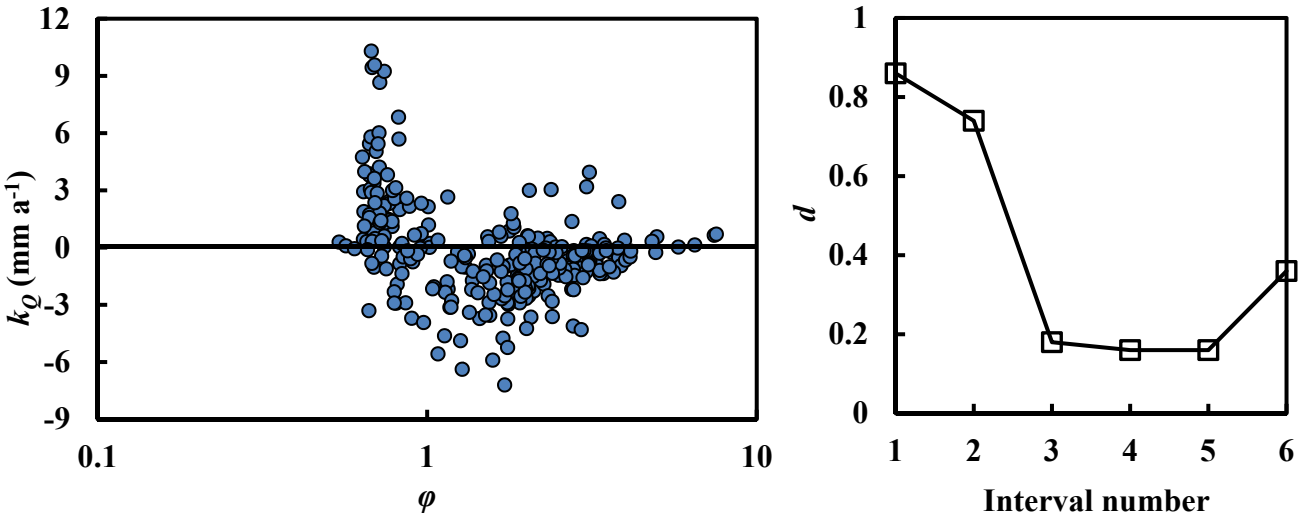

Figure 5: Relationship between observed runoff trends k_Q and mean annual runoff $\overline{Q}$ for the study catchments (left) and values of d in each interval according to φ (right). Interval numbers 1 to 6 correspond to six intervals 0.5–2/3, 2/3–1, 1–1.5, 1.5–2,2–3 and 3–8.

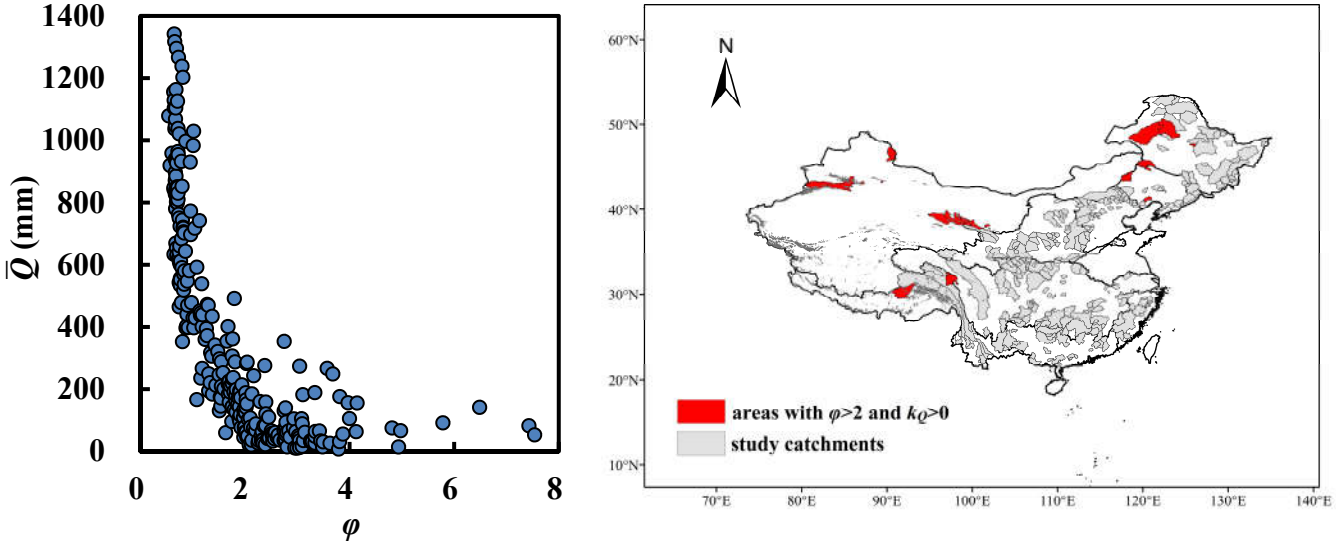

Figure 6: Relationship between mean annual runoff $\overline{Q}$ and aridity index φ in the study catchments (left) and the distribution of catchments with φ>2 and k_Q>0 (right). Grey shaded areas are glaciers based on the second glacier inventory data set of China (Guo et al., 2014).

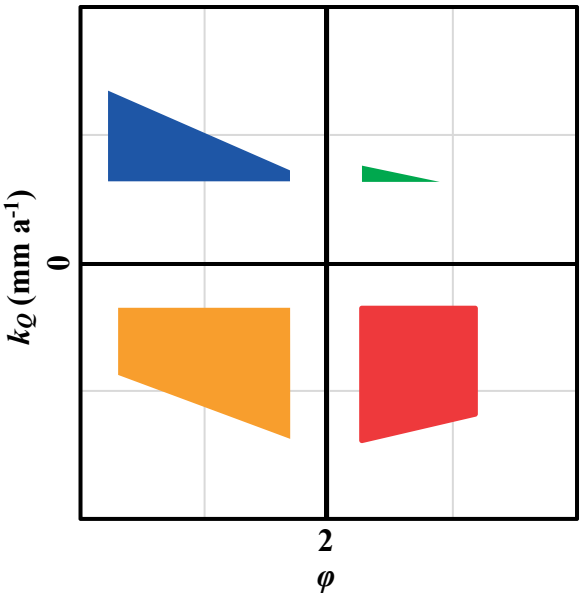

Figure 7: Diagram of a special condition of Greve et al. (2014) to make the DDWW pattern work. Blue, orange, green and red shapes denote 4 types of regions (WW, WD, DW and DD) in the previous study, with the areas denoting respective sums of each type according to the respective proportions (21%, 42%, 5% and 32%). For each shape, the area in a small interval denotes the number of respective regions, and the d of the interval is calculated by the ratio of the area of the shape over the k_Q=0 line to the total area of shape in the interval. In this situation, the DDWW pattern apparently holds, as d decreases as φ increases.

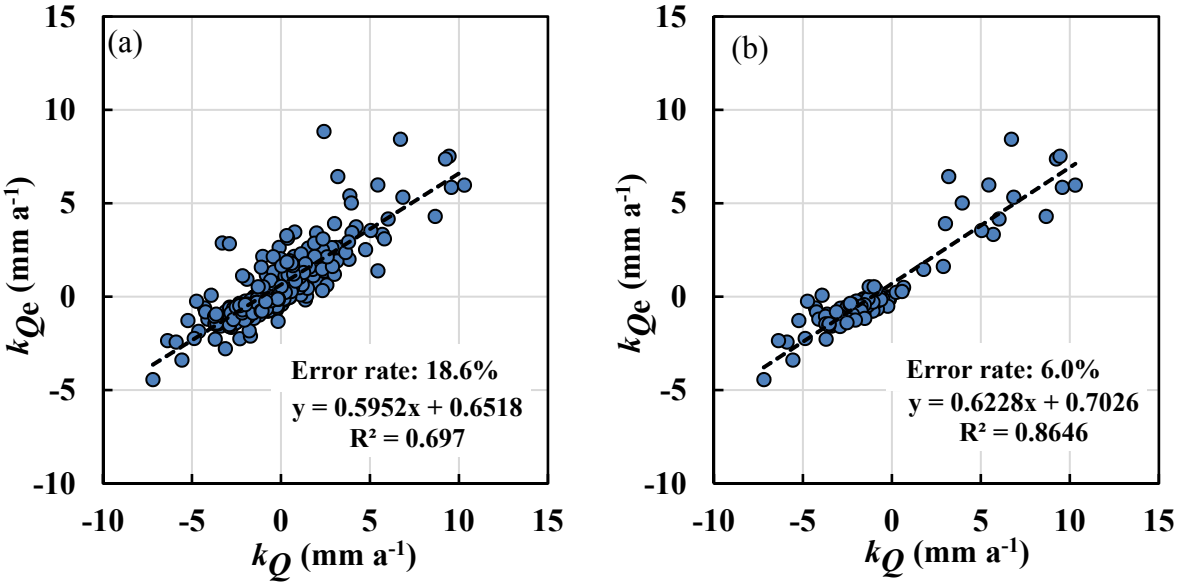

Figure 8: Comparison of estimated runoff trends k_{Qe} with observed trends k_Q for (left) all catchments and (right) significant catchments. Significant catchments are ones experiencing significant changes in runoff at the significance level of 0.05. The error rate is defined as the proportion of catchments in which the signs of the observed and estimated trends differ.

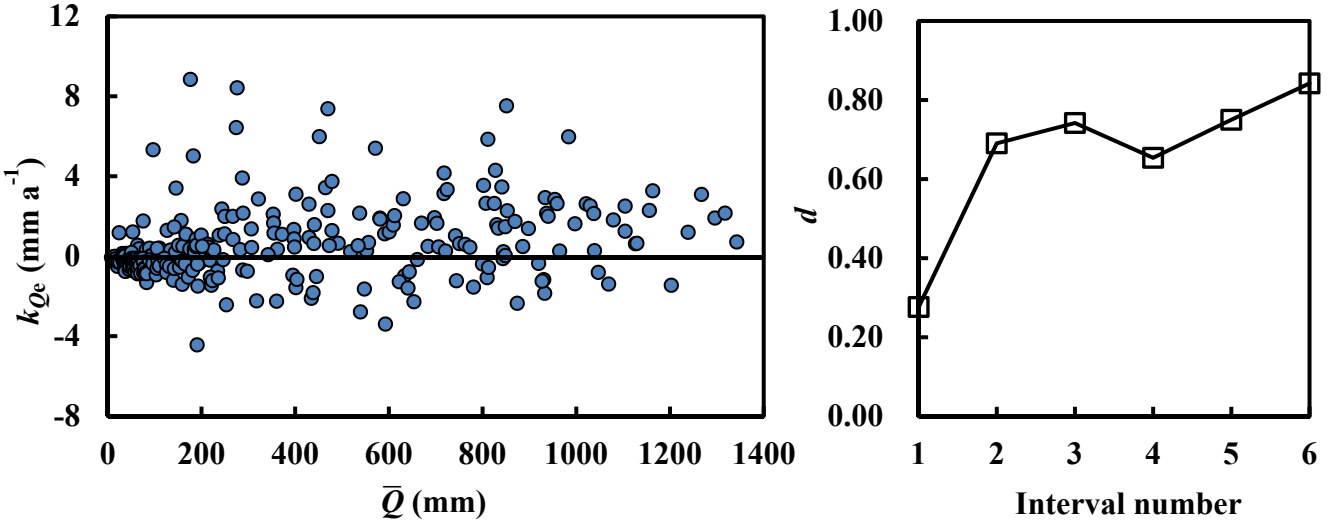

Figure 9: Relationship between observed runoff trends k_{Qe} and mean annual runoff $\overline{Q}$ for the study catchments (left) and values of d in each interval according to $\overline{Q}$ (right). Interval numbers 1 to 6 correspond to six intervals 0–200, 200–400, 400–600, 600–800,800–1000 and 1000–1400.

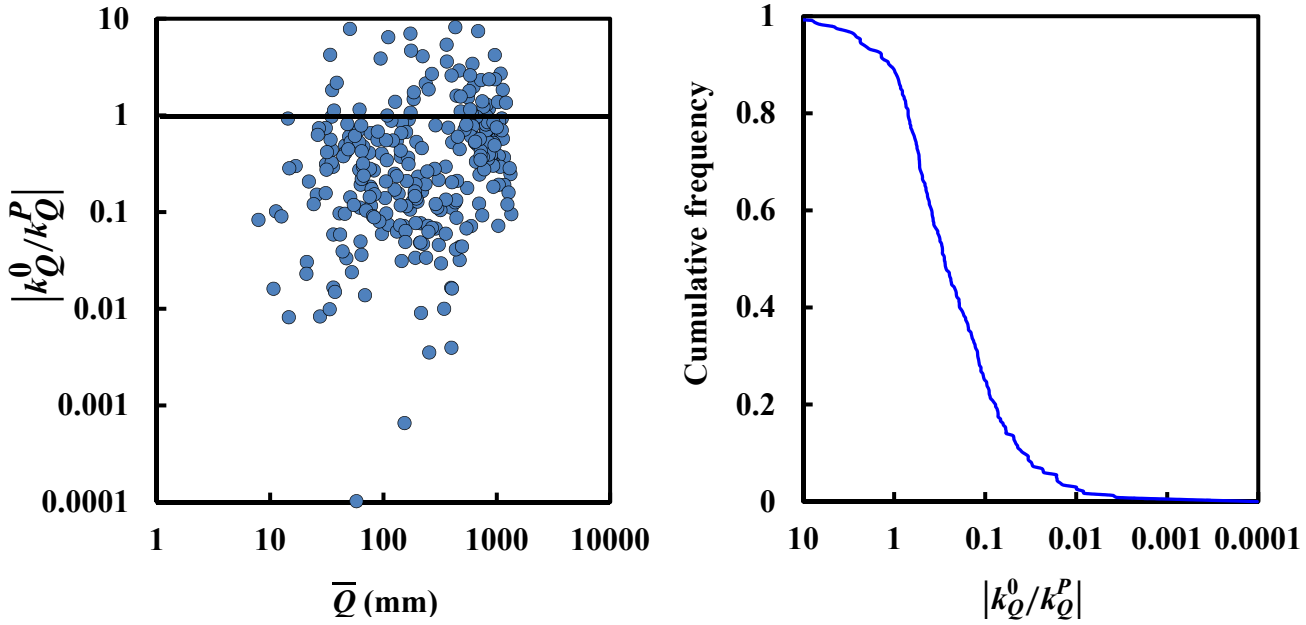

Figure 10: Exploring the controlling factor in the DDWW pattern according to the Budyko hypothesis. (left) Relationship between the ratio of absolute k_Q^0 (=$\varepsilon_0 k_{E_p}$, the part of the estimated runoff trends k_{Qe} generated from potential evapotranspiration changes**)** to absolute k_Q^P (= $\varepsilon_P k_P$, the part of k_{Qe} generated from precipitation changes) and the mean annual runoff $\overline{Q}$. **(right)** The cumulative frequency curve of $|k_Q^0/k_Q^P|$.

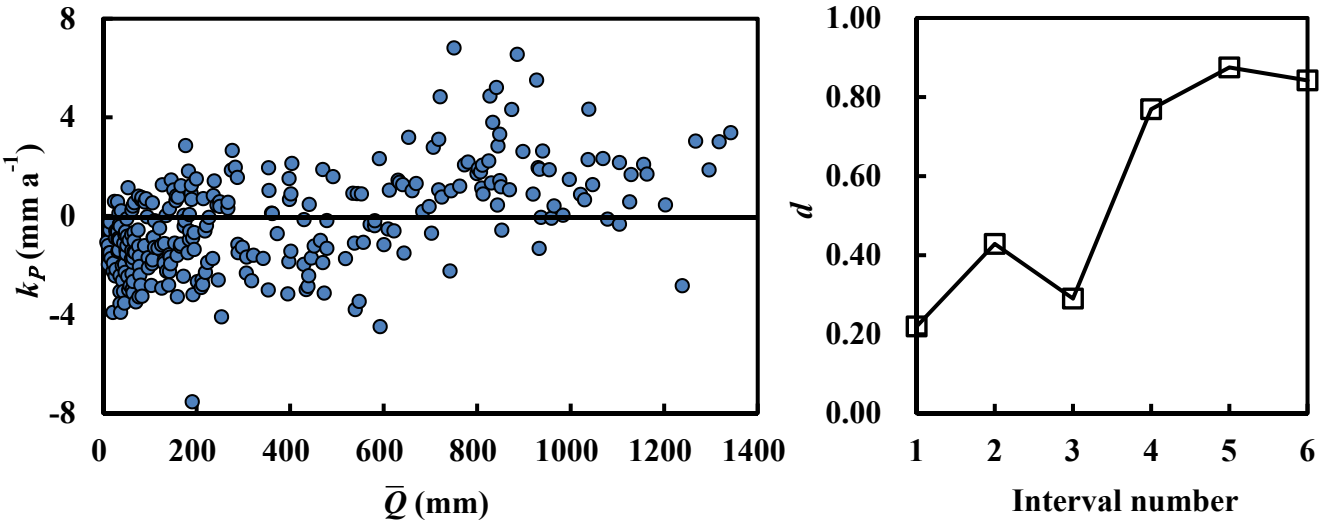

Figure 11: Relationship between observed runoff trends k_P and mean annual runoff $\overline{Q}$ for the study catchments (left) and values of d in each interval according to $\overline{Q}$ (right). Interval numbers 1 to 6 correspond to six intervals 0–200, 200–400, 400–600, 600–800,800–1000 and 1000–1400.

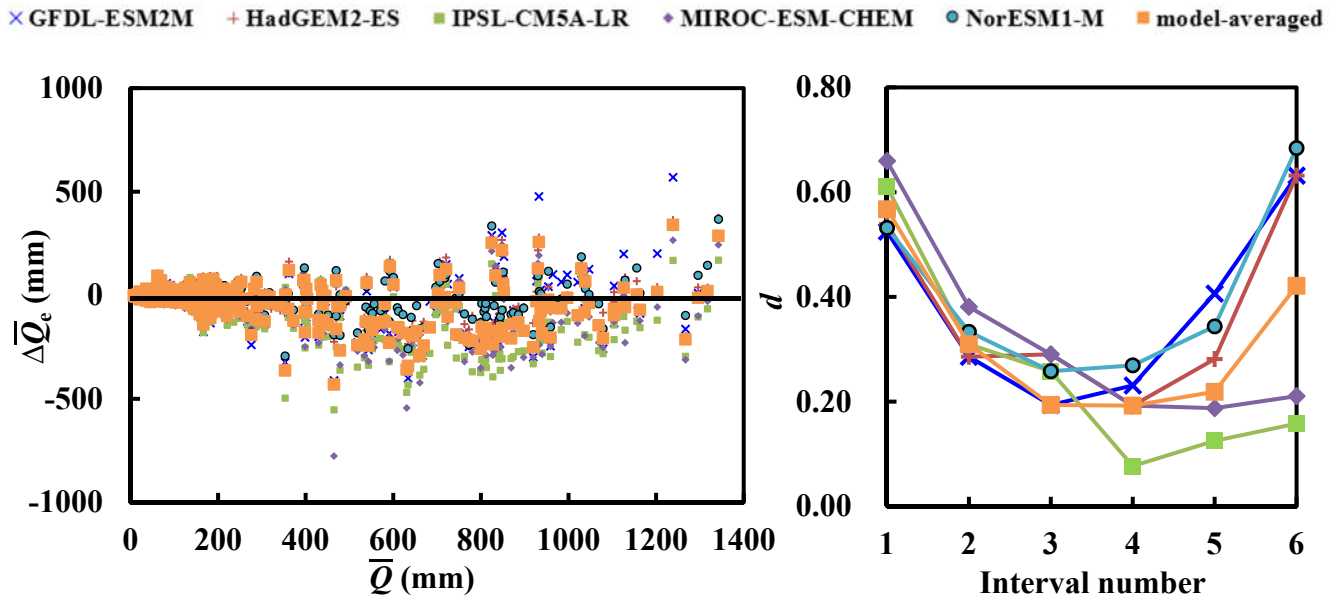

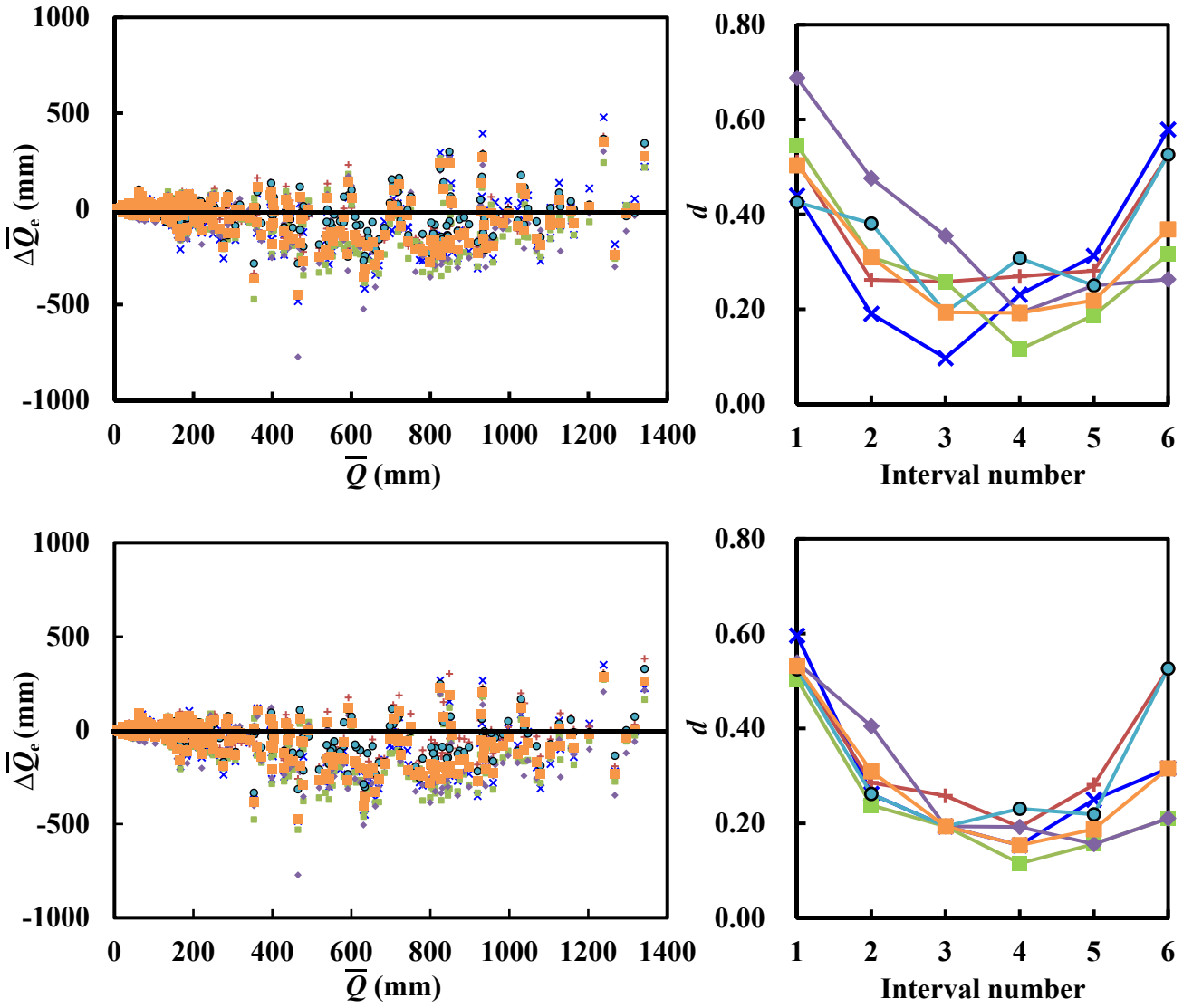

Figure 12: Projections of future trends $\Delta\overline{Q}_e$ under (top) RCP2.6, (middle) RCP4.5 and (bottom) RCP8.5 scenarios for the period 2001-2050. (left column) Relationship between projected $\Delta\overline{Q}_e$ of the five models and their means and mean annual runoff $\overline{Q}$. **(right column)** Values of d in each interval according to $\overline{Q}$ based on $\Delta\overline{Q}_e$ of the five models and their means. Interval numbers 1 to 6 correspond to six intervals 0–200, 200–400, 400–600, 600–800,800–1000 and 1000–1400.

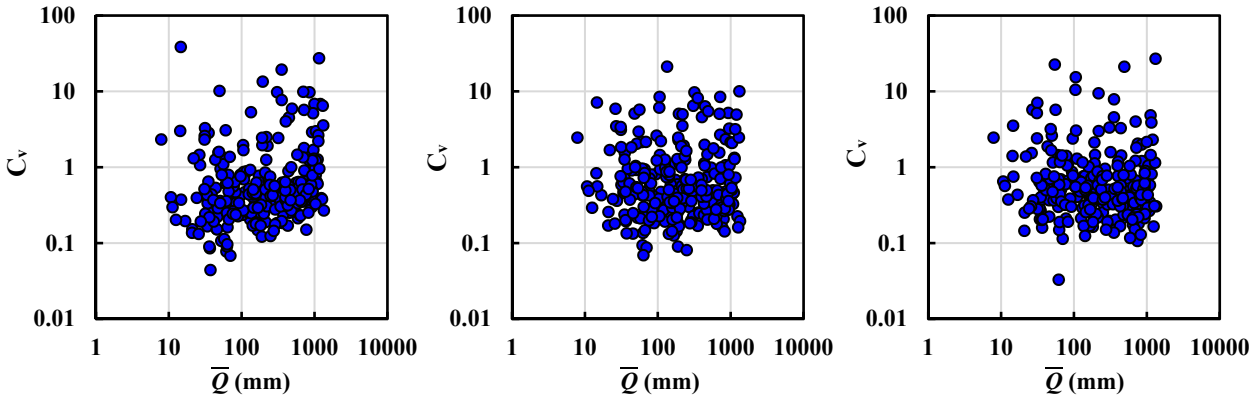

Figure 13: C_v values of projected future trends $\Delta\overline{Q}_e$ under (left) RCP2.6, (middle) RCP4.5 and (right) RCP8.5 Scenarios.

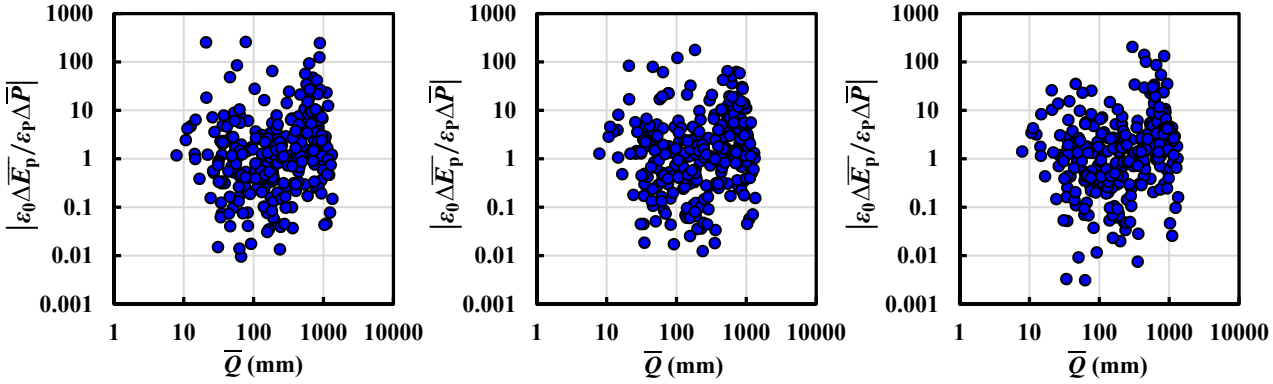

Figure 14: Exploring the controlling factor in the projected climate change under (left) RCP2.6, (middle) RCP4.5 and (right) RCP8.5.

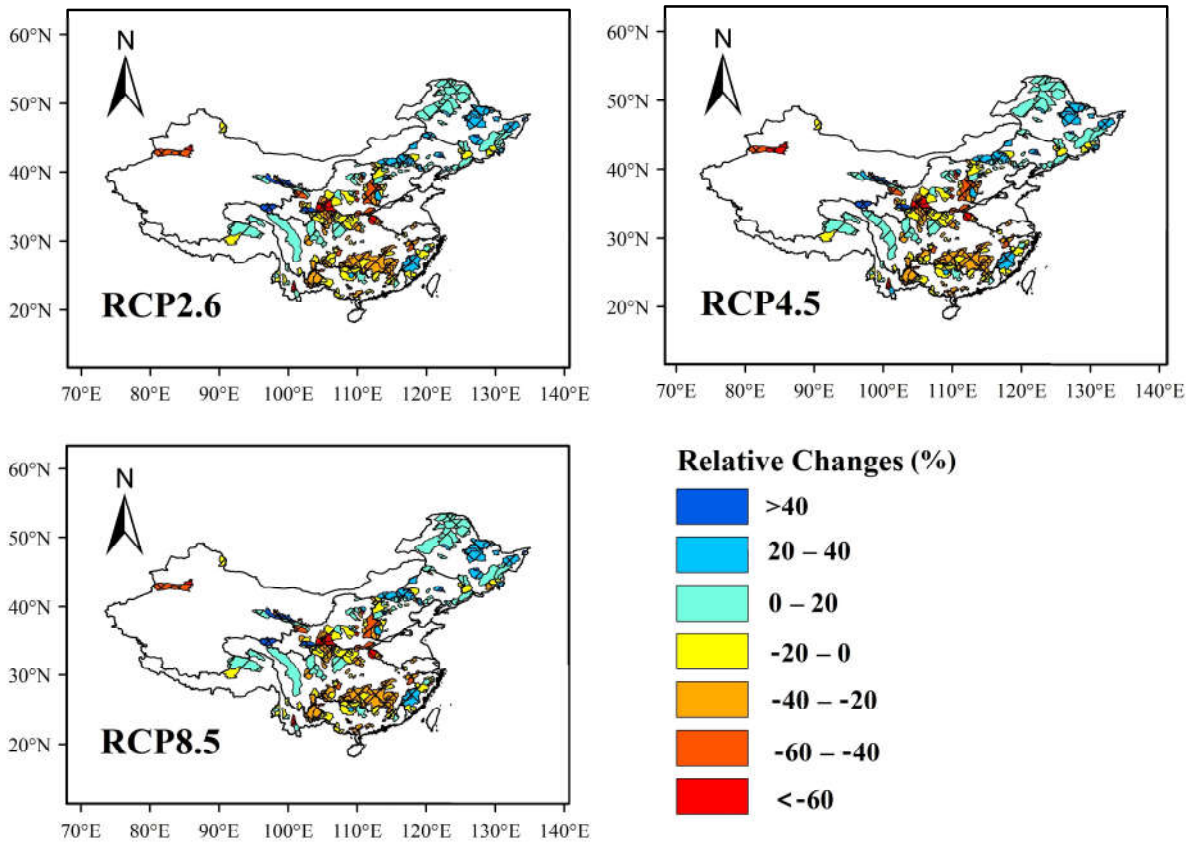

Figure 15: Spatial distribution of the model-averaged relative changes in mean annual runoff $\overline{Q}$ (=$\Delta\overline{Q}_e/\overline{Q}$) for the period of 2001 to 2050 under three different scenarios. Hatched areas denote regions with C_v values smaller than 0.5, whereas double-hatched areas represent regions with C_v values smaller than 1.

5

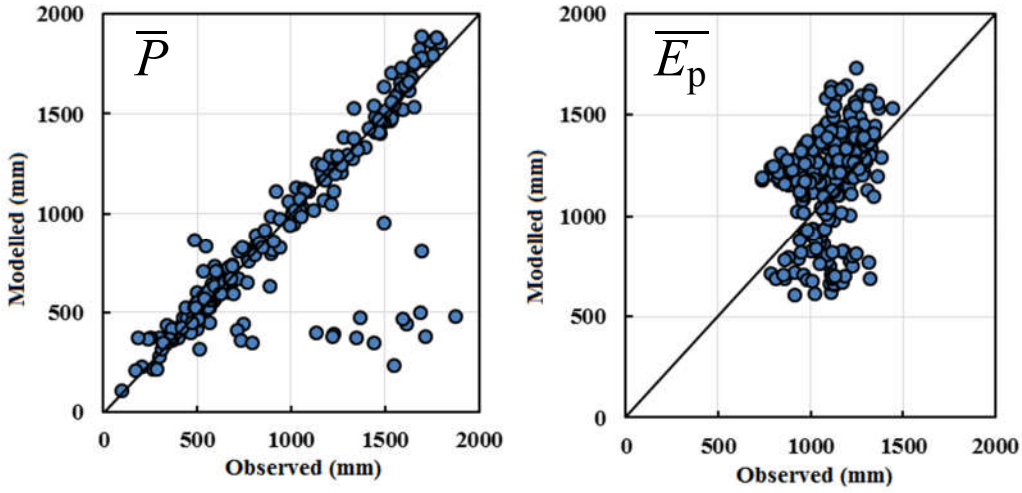

Figure 16: Comparison of the observed meteorological data with the simulations from the GFDL-ESM2M model for the period 1956–2000.

Table 1: Details of the interval partitions based on mean annual runoff $\overline{Q}$ and aridity index φ.

Interval number	Interval range	Sample size
Based on $\overline{Q}$		
1	0-200	141
2	200-400	42
3	400-600	31
4	600-800	26
5	800-1000	32
6	1000-1400	19
Based on φ		
1	0.5-2/3	21
2	2/3-1	72
3	1-1.5	33
4	1.5-2	55
5	2-3	68
6	3-8	42

Table 2: Number of catchments with k_Q>0 and respective d in each interval based on $\overline{Q}$ and φ in the analysis of the observed trends.

Interval number	Number of catchments with k_Q>0	d
Based on $\overline{Q}$		
1	26	0.18
2	11	0.26
3	12	0.39
4	20	0.77
5	28	0.88
6	15	0.79
Based on φ		
1	18	0.86
2	53	0.74
3	6	0.18
4	9	0.16
5	11	0.16
6	15	0.36

Table 3: Numbers of catchments with $\Delta\overline{Q}_e>0$ and respective *d* in each interval based on $\overline{Q}$ of five GCMs and their means in the analysis of the projected trends under three scenarios.

	Interval number	1	2	3	4	5	6
RCP2.6							
GFDL-ESM2M	Number	74	12	6	6	13	12
	d	0.52	0.29	0.19	0.23	0.41	0.63
HadGEM2-ES	Number	76	12	9	5	9	12
	d	0.54	0.29	0.29	0.19	0.28	0.63
IPSL-CM5A-LR	Number	86	13	8	2	4	3
	d	0.61	0.31	0.26	0.08	0.13	0.16
MIROC-ESM-CHEM	Number	93	16	9	5	6	4
	d	0.66	0.38	0.29	0.19	0.19	0.21
NorESM1-M	Number	75	14	8	7	11	13
	d	0.53	0.33	0.26	0.27	0.34	0.68
Model-averaged	Number	80	13	6	5	7	8
	d	0.57	0.31	0.19	0.19	0.22	0.42
RCP4.5							
GFDL-ESM2M	Number	62	8	3	6	10	11
	d	0.44	0.19	0.10	0.23	0.31	0.58
HadGEM2-ES	Number	72	11	8	7	9	10
	d	0.51	0.26	0.26	0.27	0.28	0.53
IPSL-CM5A-LR	Number	77	13	8	3	6	6
	d	0.55	0.31	0.26	0.12	0.19	0.32
MIROC-ESM-CHEM	Number	97	20	11	5	8	5
	d	0.69	0.48	0.35	0.19	0.25	0.26
NorESM1-M	Number	60	16	6	8	8	10
	d	0.43	0.38	0.19	0.31	0.25	0.53
Model-averaged	Number	71	13	6	5	7	7
	d	0.50	0.31	0.19	0.19	0.22	0.37
RCP8.5							
GFDL-ESM2M	Number	84	11	6	4	8	6

	d	0.60	0.26	0.19	0.15	0.25	0.32
HadGEM2-ES	Number	75	12	8	5	9	10
	d	0.53	0.29	0.26	0.19	0.28	0.53
IPSL-CM5A-LR	Number	71	10	6	3	5	4
	d	0.50	0.24	0.19	0.12	0.16	0.21
MIROC-ESM-CHEM	Number	76	17	6	5	5	4
	d	0.54	0.40	0.19	0.19	0.16	0.21
NorESM1-M	Number	74	11	6	6	7	10
	d	0.52	0.26	0.19	0.23	0.22	0.53
Model-averaged	Number	75	13	6	4	6	6
	d	0.53	0.31	0.19	0.15	0.19	0.32